3d transition-metal high-entropy Invar alloy developed by adjusting the valence-electron concentration

Ziyuan Rao,[1,*] Aslı Çakır ,[2] Özge Özgün ,[2] Dirk Ponge ,[1] Dierk Raabe ,[1] Zhiming Li ,[1] and Mehmet Acet[3,†]

[1]*Max-Planck-Institut für Eisenforschung GmbH, 40237 Düsseldorf, Germany*
[2]*Muğla Sıtkı Koçman University, Department of Metallurgical and Materials Engineering, 48000 Muğla, Turkey*
[3]*Faculty of Physics and Center for Nanointegration (CENIDE), Universität Duisburg-Essen, D-47048 Duisburg, Germany*

By considering the valence-electron concentration of 3d transition-metal alloys and compounds, we develop 3d high-entropy alloy $Mn_{12.1}Fe_{34.2}Co_{33.5}Ni_{12.3}Cu_{7.9}$ with 8.7 electrons per atom, which is identical to that of $Fe_{65}Ni_{35}$ Invar. We carry out x-ray diffraction, scanning electron microscopy, magnetization, thermal expansion, and elastic modulus measurements, by which we show that the HEA alloy indeed carries Invar properties. This is evidenced particularly by the observed spontaneous volume magnetostriction and the lattice softening covering a broad temperature-range around the ferromagnetic Curie temperature.

I. INTRODUCTION

As a new approach to metallic alloy design, high-entropy alloys (HEAs) are of interest due to their favorable mechanical properties such as high strength and high ductility under both cryogenic- and high-temperature conditions [1–3], and many show excellent resistance to corrosion and hydrogen embrittlement [4,5]. In contrast to the conventional alloys composed of two or three principal elements and perhaps small amounts of additional property-tuning elements, the HEAs consist of five or more elements in equimolar or near-equimolar ratios [6,7]. When in solid solution, these materials have high configurational entropy, which can be estimated from temperature-dependent heat-capacity measurements [8]. Such disordered solid solution phases mostly have simple crystallographic structures such as face-centered cubic (FCC), body-centered cubic (BCC), or hexagonal closed packed (HCP) instead of forming intermetallic phases [6]. In spite of the many beneficial mechanical properties of the HEAs, studies on their physical properties remain limited, mainly due to the complexity of their electronic structure [9–12].

The properties of 3d metals and alloys are mainly governed by their electronic structures, particularly close to the Fermi level, where s and d states are hybridized [13]. This makes it possible to view the variation of various physical properties as the number of s and d electrons vary across the 3d periodic system, this number being parameterized as the valence-electron concentration, e/a (electrons per atom). The (e/a) variation of the magnetic moment, known as the Slater-Pauling curve, is the most well-known example [14,15]. Similarly, crystallographic and magnetic transition temperatures also show universal (e/a) dependencies [16].

Magnetovolume effects in 3d metals and their alloys can also be classified in such an (e/a) scheme by considering the (e/a) dependence of the volume magnetostriction. Such a plot reveals a range of e/a, where substantial spontaneous volume magnetostriction ω_s, related to Invar and anti-Invar properties, is found with the largest magnetovolume effects occurring around $(e/a) = 8.7$ for Invar and around $(e/a) = 7$ for anti-Invar [16].

In a similar manner, the physical properties of HEAs composed of only 3d elements can also be expected to show universal behavior with respect to e/a. For example, the equiatomic CrMnFeCoNi Cantor high-entropy alloy with fcc structure has $(e/a) = 8$, which is the same value for Fe. However, the structure of CrMnFeCoNi at room temperature is not BCC but instead FCC throughout the solid-state temperature range. This feature makes CrMnFeCoNi particularly interesting because at this (e/a) value, one can expect that the alloy would exhibit the predicted anti-Invar properties of FCC-Fe, which is discussed in the subsequent paragraph. Indeed, recent studies have shown that the Cantor alloy shows similar anti-Invar properties [17].

Invar is the unique property of a material having a low coefficient of thermal expansion α because of the presence of magnetovolume fluctuations occurring between the large-volume-high-moment ground state and the energetically higher-lying small-volume-low-moment state [16,18,19]. Anti-Invar is just the opposite of this, whereby the large-volume-high-moment state is the energetically higher-lying state than the equilibrium small-volume-low-moment state [20,21]. In the case of Invar, the presence of these states provides a quasinegative anharmonicity allowing at finite temperatures the small-volume-low-moment state to be progressively accessed through high-moment to low-moment fluctuations. The quasinegative anharmonicity compensates the normal positive anharmonicity, and the material does not expand. The prototype material with $(e/a) = 8.7$ is the $Fe_{65}Ni_{35}$ alloy, which exhibits a small thermal expansion coefficient ranging from

*z.rao@mpie.de
†mehmet.acet@uni-due.de

low temperatures up to its magnetic transition temperature at around 550 K [16]. In the case of anti-Invar, the normal positive anharmonicity is enhanced, and the material expands more than normal. Invar and anti-Invar materials can be both ferromagnetic and antiferromagnetic in their ground states. Both effects rely on high-moment-to-low-moment fluctuations.

Just as the anti-Invar effect can be found in a HEA, it should also be possible to design an Invar-HEA by adjusting its e/a. Therefore, composing a HEA with $(e/a) \approx 8.7$ could be a suited design pathway for an alloy with a magnetovolume effect over a considerable temperature range and should also show a lattice softening in the temperature range where the magnetovolume effect occurs. For a normal metallic material, decreasing the temperature causes a volume decrease, and the elastic modulus increases accordingly. For Invar materials, the volume expansion is compensated by the quasinegative anharmonicity in the ground state resulting in a decrease in the elastic modulus with decreasing temperature [22]. The details of lattice softening can be found in the results of extended x-ray absorption fine structure studies [23]. In some cases, the elastic modulus can be temperature independent over a broad temperature, which is known as the Elinvar effect. In this work, we design a HEA with $(e/a) = 8.7$ and investigate it using x-ray diffraction (XRD), thermal expansion, magnetization, and elastic properties measurements. We verify that based on the (e/a) scheme, the material does indeed exhibit Invar properties as we evidence from the results of measurements on the temperature dependencies of the thermal expansion and the Young's modulus.

II. EXPERIMENTAL

An ingot of $Mn_{12.1}Fe_{34.2}Co_{33.5}Ni_{12.3}Cu_{7.9}$ HEA [composition in at.% and elements arranged in increasing valence-electron concentration (e/a)], for which (e/a) is the same as that for $Fe_{65}Ni_{35}$ with $(e/a) = 8.70$), was prepared in a vacuum induction furnace using pure metals with purity of at least 99.8%. The composition was determined by wet-chemical analysis. A sample with dimensions $25 \times 60 \times 10 \text{ mm}^3$ was machined from the cast ingot and homogenized at $1000\,^\circ$C for 24 h in Ar atmosphere followed by water quenching.

The microstructures of the as-cast and homogenized samples were analyzed using XRD and scanning electron microscopy (SEM). XRD was performed with an ISODE-BYEFLEX 3003 instrument using Co Kα radiation. Electron backscatter diffraction (EBSD) measurements were performed with a Zeiss-Crossbeam XB 1540 focused ion beam scanning electron microscope (SEM) with a Hikari camera and TSL OIM data-collection software. Back-scattered electron imaging (BSEI) was carried out on a Zeiss-Merlin instrument. Energy-dispersive X-ray spectroscopy (EDS) was used to study the elemental distributions at the microscale. Before the microstructural analysis, we carried out fine polishing of the surfaces using an oxide polishing suspension (OPS) with 50 nm silica particles for 30 minutes to effectively remove the deformation layer caused by mechanical grinding. The sample surfaces were finally cleaned with soap and ethanol for 5 minutes to remove the silica particles.
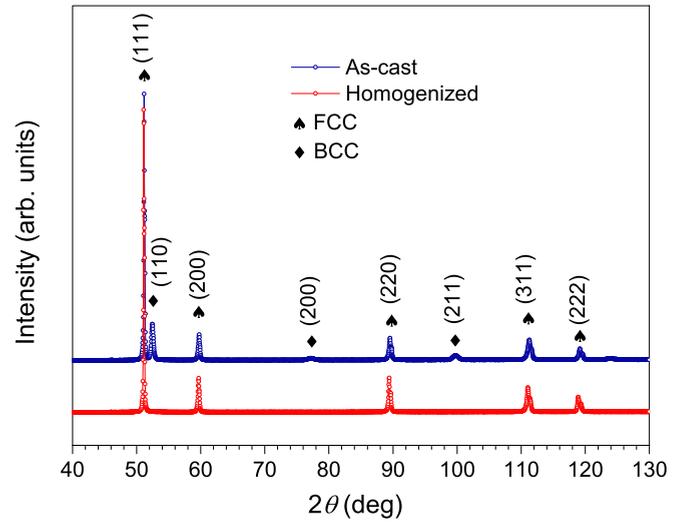
FIG. 1. XRD patterns for the as-cast (blue) and homogenized samples (red). The as-cast pattern shows both BCC and FCC peaks as well as some faint unidentified peaks, e.g., 124°. Only FCC peaks are observed for the homogenized sample.

Magnetization measurements were carried out using a physical properties measurement system (PPMS) from Quantum Design, which is equipped with a vibrating sample magnetometer. The temperature and field dependencies of the magnetization, $M(T)$ and $M(B)$, were measured in the ranges $300 \leqslant T \leqslant 900$ K and $0 \leqslant B \leqslant 9$ T, respectively.

The thermal expansion of the homogenized sample was measured in the range $5 \leqslant T \leqslant 900$ K. The range $5 \leqslant T \leqslant 400$ K was covered in the PPMS using a dilatometer insert having a resolution of 0.02 Å. A thermal dilatometer, with the sample under argon atmosphere, was used for the range $400 \leqslant T \leqslant 900$ K. The resolution in this case is 0.1 Å. In both cases the heating rate was 1 K min^{-1}. The thermal expansion coefficient $\alpha(T)$ was determined from the data.

The temperature dependence of the Young's modulus (elastic modulus), $E(T)$ was performed using the impulse excitation technique (IET) [24]. The IET has the advantage of being a nondestructive and relatively faster method for determining the Young's modulus than other conventional methods. The measurement was performed in the range $300 \leqslant T \leqslant 900$ K with a 1 K min^{-1} heating rate.

III. RESULTS

Figure 1 shows the XRD patterns of the as-cast and homogenized samples. The as-cast alloy contains both FCC and BCC structures while the homogenized alloy has a single FCC structure. The lattice parameters of the FCC and BCC phases in the as-cast alloy are found by Rietveld refinement to be 0.3596 and 0.2870 nm, respectively. The lattice parameter of the homogenized alloy is 0.3595 nm, similar to that of the FCC phase in the as-cast state.

Figure 2 shows the EBSD maps, BSE images, and the corresponding EDS maps of the as-cast and homogenized alloys. Fig. 2(a) shows the BSE, the inverse pole figure (IPF), and phase maps of the as-cast alloy. The as-cast alloy shows both FCC (red) and BCC (green) phases which is consistent
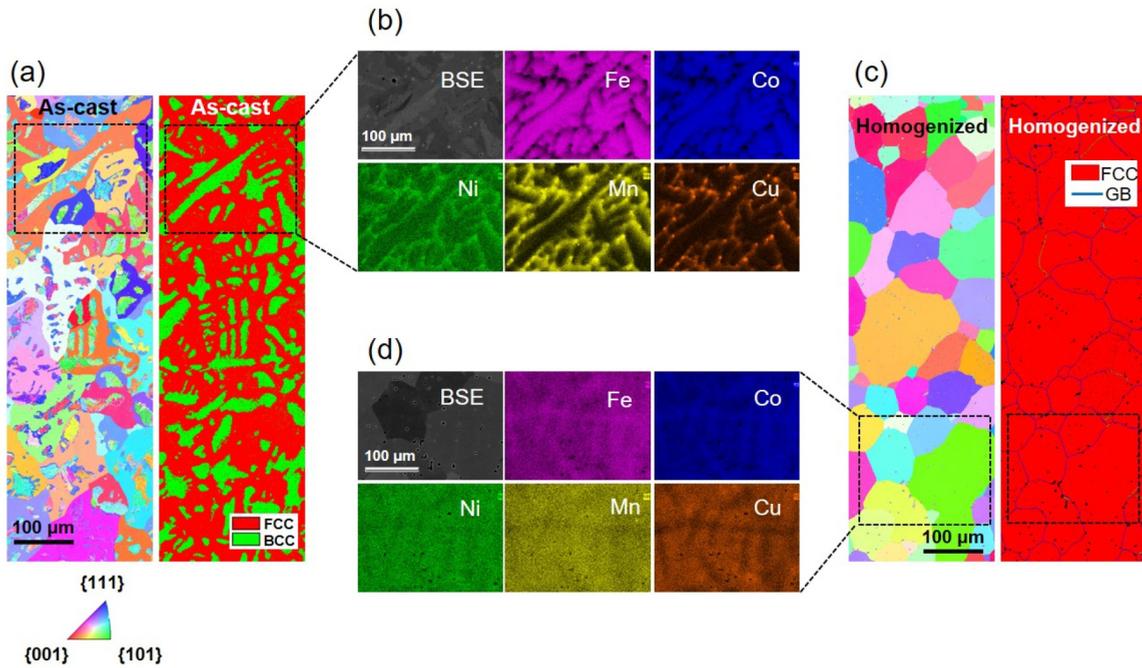
FIG. 2. Microstructure and elemental distribution of the as-cast and homogenized state. (a) EBSD IPF and phase maps of the as-cast alloy, (b) the BSE image and corresponding EDS maps of Fe, Ni, Co, Mn and Cu of the region marked in (a). (c) EBSD IPF, phase and boundary maps of the homogenized sample, (d) BSE image of the homogenized alloy and corresponding EDS maps of Fe, Ni, Co, Mn and Cu with an identical sample region marked in (c).

with the XRD results. The grain orientation is color coded. The grain size of the FCC and BCC phases are around 100 and 15 μm, respectively. The fraction of the FCC phase is 71%. Figure 2(b) shows the BSE image and the corresponding EDS maps of the as-cast alloy. Typical dendritic microstructures can be observed. The EDS maps show that the dendrite arms are enriched in Cu, Mn and Ni while the interdendritic regions are mainly BCC and enriched in Fe and Co. Therefore, the interdendritic regions can be expected to be an Fe-Co alloy, which would be compatible with the observed BCC lattice-constant value of $a = 2.870$ Å.

Figure 2(c) shows the BSE, IPF, and phase and grain-boundary maps of the homogenized sample. During homogenization, the alloy recrystallizes and acquires a grain size of about 95 μm (excluding annealing twin boundaries). Figure 2(d) shows that all the elements are almost uniformly distributed. Some inhomogeneity can still be observed especially in the Cu map. This is commonly found in Cu-containing HEA systems [25,26]. Nevertheless, the quite random distribution of the elements is supporting evidence for labeling these alloys as being of high entropy.

Figure 3 shows the results of the magnetization measurements of the homogenized sample. $M(T)$ measured in a small field of 10 mT yields a sharp change at 509 K, which is identified as the Curie temperature T_C [Fig. 3(a)]. $M(B)$ measured at 300 K (inset) gives a saturation magnetization M_s of 83.9 Am^2 kg^{-1}. This gives an average magnetic moment, $\mu = 0.9$ μ_B per atom, which corresponds to a value lying within the Invar region of Fe-Ni alloys [21]. Figure 3(b) compares the dependence of the reduced saturation magnetization M/M_0, where M_0 is the saturation magnetization at low temperature on the temperature reduced

to T_C, T/T_C. M/M_0 vs T/T_C is essentially a Brillouin curve and complies to the mean-field model. In Invar alloys M/M_0 decreases more rapidly than that predicted by the mean-field model [27]. M/M_0 vs T/T_C for the present alloy shows a behavior that is indeed similar to Invar alloys.

Figure 4 shows $\alpha(T)$ (blue) and $E(T)$ of the homogenized alloy. The dashed blue line represents the regular lattice expansion for cubic 3*d* metals and alloys [28], and the heavy blue line is the expansion of the sample. The area enclosed between these two lines is the spontaneous volume magnetostriction, $\omega_s = 3\Delta l/l = 0.2 \times 10^{-2}$, where $\Delta l/l$ is the length change. The volume magnetostriction covering approximately the range $200 \leqslant T \leqslant 800$ K is an indication of the presence of the Invar effect. At temperatures well above T_C, $\alpha(T)$ follows a regular lattice-expansion behavior. Some deviations from the regular lattice behavior occur at temperatures above 800 K. This can be due to a secondary annealing effect at these temperatures resulting in the formation of new phases, thereby affecting $\alpha(T)$. This is commonly observed in HEAs [29]. The inset focuses on $\alpha(T)$ in the range $5 \leqslant T \leqslant 65$ K, where a shallow minimum in the curve around 30 K can be noticed. This feature, which is present in Invar materials, is caused by an intrinsic strain due to mixed magnetic interactions that freeze-in when cooling the sample to low temperatures [30]. Due to the magnetoelastic coupling the strain also freezes. The frozen strain causes the retainment of an atomic volume which is slightly larger than what it would be expected to be at low temperatures. When measuring the thermal expansion on increasing temperature, the strain is slowly released, and the volume relaxes to a lower volume. This causes $\alpha(T)$ to attain negative values and to show a minimum at low temperatures.
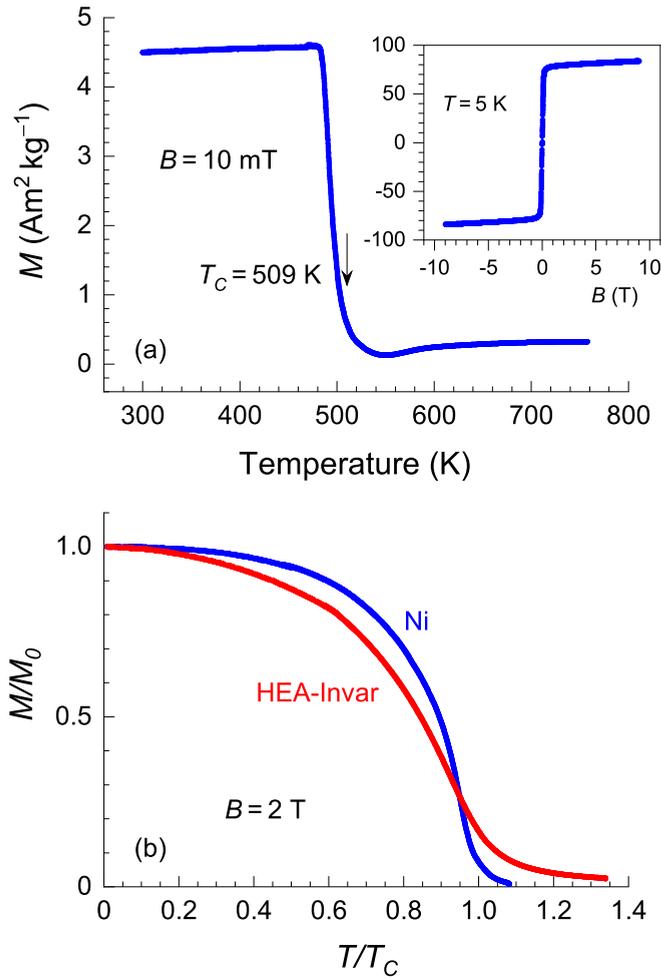
FIG. 3. The magnetization studies. (a) $M(T)$ of the homogenized sample for $300 \leqslant T \leqslant 900$ K measured in 10 mT. The inset shows $M(B)$ at 5 K. (b) M/M_0 vs T/T_0 for homogenized Invar-HEA and Ni. The faster decrease of M/M_0 with increasing temperature with respect to that of Ni, which follows Brioullin behavior, is typical of Invar alloys.

An important feature of the Invar effect is that an Invar material exhibits softening in the temperature range covered by the volume magnetostriction. The softening can be readily observed in the temperature dependence of the bulk modulus or the Young's modulus. A decrease in the magnitude of these parameters with decreasing temperature occurs in a broad temperature range around T_C. To provide further evidence for the occurrence of the Invar effect in the present HEA, we measured $E(T)$. This is plotted as the solid red line in Fig. 4. As can be seen $E(T)$ shows a decrease around T_C with decreasing temperature and remains at lower values with respect to the red dashed curve, which $E(T)$ would have followed in the absence of the Invar effect. The area enclosed between the data and the dashed line is the spontaneous softening due to the Invar effect. The softening would have been more accurately determined if the bulk modulus B were determined as a function of temperature rather than E. In this case, the temperature range of the softening determined by $B(T)$ would match the range of the anomaly in $\alpha(T)$, since the bulk modu-
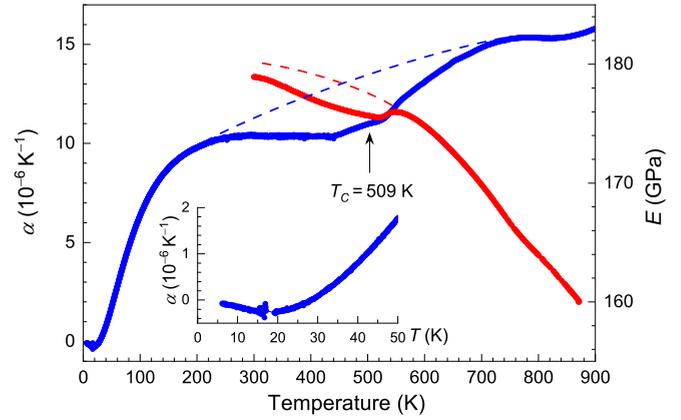
FIG. 4. The thermal expansion coefficient $\alpha(T)$ (blue) and the elastic modulus $E(T)$ (red) of the homogenized $Mn_{12.1}Fe_{34.2}Co_{33.5}Ni_{12.3}Cu_{7.9}$ high-entropy alloy. The dashed lines denote the regular lattice expansion (blue) and the regular elastic-modulus change. The deviations from these regular behaviors are due to the Invar effect. The inset shows a minimum occurring in $\alpha(T)$ at low temperatures that is commonly observed in Invar-type alloys.

lus is a parameter related to a volume change like the isotropic thermal expansion coefficient. However, measuring the bulk modulus is more cumbersome due to the use of pressure cells,
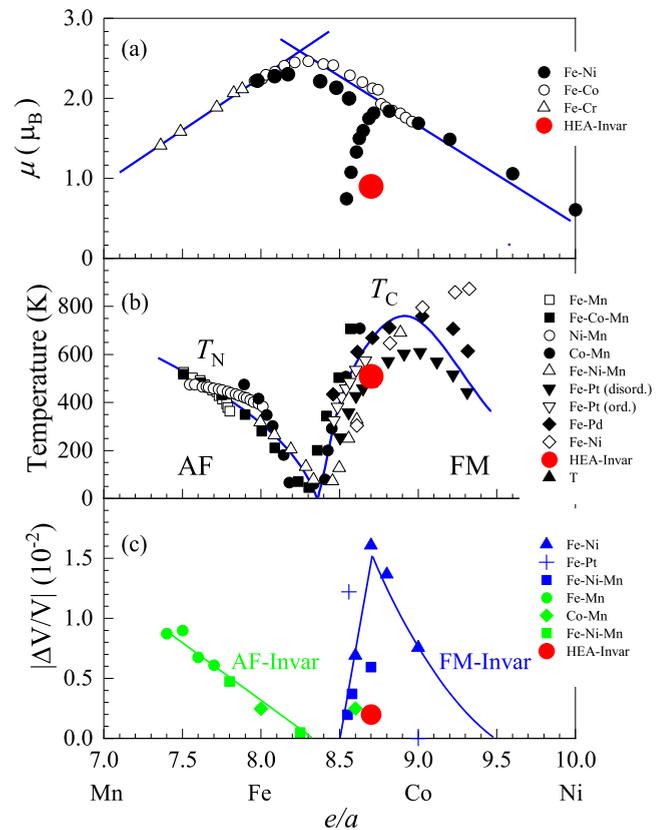
FIG. 5. The (e/a) dependence of various physical parameters for $3d$ alloys. (a) The average magnetic moment, (b) the magnetic transition temperatures, and (c) the spontaneous volume magnetostriction. The large red symbols are the values for the present HEA alloy. Blue and green lines are guides.

and for the present purpose of demonstrating the presence of Invar-softening, determining $E(T)$ by using the fast IET method is a compromising alternative.

IV. DISCUSSION

The (e/a) dependence of physical parameters in $3d$ alloys and compounds can reveal universal properties, and it can be expected that HEAs should fit into the (e/a) scheme. We therefore compare the parameters μ, T_C, and the spontaneous volume magnetostriction ω_s. These are collected in Fig. 5. Figure 5(a) shows the Slater-Pauling curve in the (e/a) region particularly where Invar effects are observed in Fe-Ni alloys as a deviation from the curve. The position of the heavy red data point, corresponding to μ of the present Invar-HEA, is in agreement with the deviation from the Slater-Pauling curve.

In Fig. 5(b), we plot the Néel temperatures T_N and the T_Cs of antiferromagnetic and ferromagnetic Invar-type alloys. Here also it can be seen that T_C of the Invar-HEA takes up a position on the curve that is in agreement with the T_Cs of the ferromagnetic Invar alloys.

The case is not as clear for ω_s as it is for μ and the magnetic transition temperatures. ω_s for this composition should lie at values closer to that of the $Fe_{65}Ni_{35}$ value, namely around 1–1.5×10^{-2}, but it lies in fact much lower at about 0.2×10^{-2}. Although the sample has undergone a homogenization heat treatment, we have seen that some inhomogeneities are still present in the elemental distribution as seen in Fig. 2(d), although the material is in a single-phase FCC. There are regions in the sample that have e/a close to 8.7 which contribute with Invar properties and those that are far from 8.7 that hinder Invar properties; even though the average e/a is 8.7. Nevertheless, it appears that the homogeneity of the sample is sufficient for μ and T_C to take up positions that are in general agreement with the (e/a) scheme. However, with inhomogeneities counteracting the Invar effect, the whole of the sample cannot exhibit fully the Invar effect with a large ω_s. Regions that are far from the $(e/a) = 8.7$ concentration will act to suppress the Invar effect by increasing the thermal expansion. Therefore, a higher ω_s can be expected for a sample with a higher degree of homogeneity. Works aiming to improve the homogeneity of such systems would be useful to understand better the basic properties of $3d$ HEAs.

V. CONCLUSIONS

Using the (e/a) scheme for $3d$ alloys and compounds we have shown that it is possible to design materials with desired Invar properties. We prepared a Mn-Fe-Co-Ni-Cu HEA with $(e/a) = 8.7$, which corresponds to that of the Invar-alloy $Fe_{65}Ni_{35}$, and demonstrated that it indeed carries Invar properties. The results also suggest that improving the homogeneity would improve the low thermal-expansion and elastic properties. The study thus presents a method to identify new alloy variants that could combine advanced functional properties such as Invar with other beneficial features that have before been identified for entropy alloys, such as high mechanical strength or good corrosion properties.

[1] Y. Zou, H. Ma, and R. Spolenak, Nat. Commun. **6**, 7748 (2015).

[2] B. Gludovatz, A. Hohenwarter, D. Catoor, E. H. Chang, E. P. George, and R. O. Ritchie, Science **345**, 1153 (2014).

[3] H. Kou, J. Lu, and Y. Li, Adv. Mater. **26**, 5518 (2014).

[4] C. P. Lee, Y. Y. Chen, C. Y. Hsu, J. W. Yeh, and H. C. Shih, J. Electrochem. Soc. **154**, C424 (2007).

[5] H. Luo, W. Lu, X. Fang, D. Ponge, Z. Li, and D. Raabe, Mat. Today **21**, 1003 (2018).

[6] J. W. Yeh, S. K. Chen, S. J. Lin, J. Y. Gan, T. S. Chin, T. T. Shun, C. H. Tsau, and S. Y. Chang, Adv. Eng. Mater. **6**, 299 (2004).

[7] B. Cantor, I. T. H. Chang, P. Knight, and A. J. B. Vincent, Mater. Sci. Eng. A **375-377**, 213 (2014).

[8] S. Haas, M. Mosbacher, O. N. Senkov, M. Feuerbacher, J. Freudenberger, S. Gezgin, R. Völkl, and U. Glatzel, Entropy **20**, 654 (2018).

[9] J. Guo, H. Wang, F. von Rohr, Z. Wang, S. Cai, Y. Zhou, K. Yang, A. Li, S. Jiang, R. J. Cava, and L. Sun, Proc. Natl. Acad. Sci. **114**, 13144 (2017).

[10] P. Kozelj, S. Vrtnik, A. Jelen, S. Jazbec, Z. Jaglicic, S. Maiti, M. Feuerbacher, W. Steurer, and J. Dolinsek, Phys. Rev. Lett. **113**, 107001 (2014).

[11] L. Liu, S. Huang, L. Vitos, M. Dong, E. Bykova, D. Zhang, B. S. G. Almqvist, S. Ivanov, J. Rubensson, B. Varga, L. K. Varga, and P. Lazor, Commun. Phys. **2**, 42 (2019).

[12] Y. Zhang, T. Zuo, Y. Cheng, and P. K. Liaw, Sci. Rep. **3**, 1455 (2013).

[13] J. C. Slater, Phys. Rev. **36**, 57 (1930).

[14] J. C. Slater, Phys. Rev. **49**, 931 (1936).

[15] L. Pauling, Phys. Rev. **54**, 899 (1938).

[16] E. F. Wassermann, in *Ferromagnetic Materials*, Vol. 5 (Elsevier, Amsterdam, 1990), pp. 238–322.

[17] M. Acet, AIP Adv. **9**, 095037 (2019).

[18] V. L. Moruzzi, Phys. Rev. B **39**, 6957 (1989).

[19] V. L. Moruzzi, Phys. Rev. B **41**, 6939 (1990).

[20] M. Acet, H. Zähres, E. F. Wassermann, and W. Pepperhoff, Phys. Rev. B **49**, 6012 (1994).

[21] W. Pepperhoff and M. Acet, *Constitution and Magnetism of Iron and its Alloys, Engineering Materials and Processes* (Springer, Berlin, 2001).

[22] Ph. Renaud and S. G. Steinemann, Physica B **161**, 75 (1990).

[23] M. Kousa, S. Iwasaki, N. Ishimatsu, N. Kawamura, R. Nomura, S. Kakizawa, M. Mizumaki, H. Sumiya, and T. Irifune, High Pressure Res. **40**, 130 (2020).

[24] G. Roebben, B. Basu, J. Vleugels, J. V. Humbeeck, and O. V. der Biest, J. Alloys Compd. **310**, 284 (2000).

[25] Z. Rao, B. Dutta, F. Körmann, Dirk Ponge, L. Li, J. He, L. Stephenson, L. Schäfer, K. Skokov, O. Gutfleisch, D. Raabe, and Z. Li, Phys. Rev. Materials **4**, 014402 (2020).

[26] Z. Rao, B. Dutta, F. Körmann, W. Lu, X. Zhou, C. Liu, A. Kwiatkowski da Silva, U. Wiedwald, M. Spasova, M. Farle, D. Ponge, B. Gault, J. Neugebauer, D. Raabe, and Z. Li, Adv. Func. Mater. **31**, 2007668 (2020).

[27] S. F. Dubinin, S. K. Sidorov, and E. Z. Valiev, phys. stat. sol. (b) **46**, 337 (1971).

[28] E. F. Wassermann, M. Acet, P. Entel, and W. Pepperhoff, J. Magn. Soc. Jpn. **23**, 385 (1999).

[29] N. D. Stepanov, D. G. Shaysultanov, M. S. Ozerov, S. V. Zherebtsov, and G. A. Salishchev, Mat. Lett **185**, 1 (2016).

[30] H. Zähres, M. Acet, W. Stamm, and E. F. Wassermann, J. Magn. Magn. Mater. **72**, 80 (1988).